

HI Absorption Toward the Nucleus of the Radio Galaxy PKS 2322–123 in A 2597

G. B. Taylor¹, C. P. O’Dea², A. B. Peck^{1,3}, & A. M. Koekemoer²

ABSTRACT

We present sensitive, high resolution Very Long Baseline Array (VLBA) observations of the central $0.3''$ of PKS 2322–123 at 1.3 and 5 GHz. These observations reveal straight and symmetric jets emerging from both sides of an inverted spectrum core. The 21 cm line of atomic hydrogen is detected in absorption against the core and eastern jet with substantial opacities, but is not seen towards the equally strong western jet. Both a narrow (110 km s^{-1} FWHM) and a very broad (735 km s^{-1} FWHM) line are seen, although the very broad line is seen only against the core. Both lines are redshifted ($\sim 220 \pm 100 \text{ km s}^{-1}$) with respect to the systemic velocity. The most likely explanation for the observed HI kinematics are an atomic torus centered on the nucleus with considerable turbulence and inward streaming motions. The scale height of this torus is less than 20 pc. Though rare in flux limited samples of compact radio sources, symmetric parsec-scale structure appears nearly ubiquitous among radio galaxies with HI absorption, probably because they are viewed more nearly edge-on through the torus.

Subject headings: cooling flows — galaxies: clusters: individual (A 2597) — galaxies: jets — radio continuum:galaxies — galaxies:elliptical and lenticular, cD: — radio lines: galaxies — galaxies:individual (PKS 2322–123)

¹National Radio Astronomy Observatory, Socorro, NM 87801, USA; gtaylor@nrao.edu, apeck@nrao.edu

²Space Telescope Science Institute, Baltimore, MD 21218, USA; odea@stsci.edu, koekemoer@stsci.edu

³New Mexico Institute of Mining and Technology, Socorro, NM 87801, USA

1. Introduction

HI gas has now been detected towards several radio galaxies embedded in X-ray cooling flow clusters: 3C 84 in A 426 (Crane et al. 1982; Jaffe 1990); Hydra A in A 780 (Taylor 1996; Dwarakanath, Owen, & van Gorkom 1995), and recently PKS 2322–123 in A 2597 (O’Dea, Baum & Gallimore 1994). In an even larger number of such radio galaxies HI has not been detected in spite of fairly intensive searches (e.g. Virgo A, and 3C 338 in A 2199 – Dwarkanath, van Gorkom, & Owen 1994; Jaffe 1991; O’Dea, Gallimore, & Baum 1995). Besides a natural curiosity about these unusual systems, additional motivation to search for HI has come from the discovery of excess low-energy X-ray absorption (White et al. 1991) which has been suggested to be due to a population of cold HI clouds in the cluster with a column density of $N_{\text{H}} \sim 10^{21} \text{ cm}^{-2}$ and covering factor near unity. To date this population has not been seen and the HI gas that is detected seems to be closely associated with the active nucleus. In Hydra A the HI gas appears to be distributed in a disk having a rotation axis closely aligned with the jet axis and with a height of just 30 pc.

O’Dea, Baum & Gallimore (1994) detected two HI components in PKS 2322–123 using the VLA in its A configuration. One component is a narrower (220 km s^{-1} wide) feature seen only towards the center of the source (the location of the nucleus). The other component is broader (410 km s^{-1} wide) and spatially extended against the entire radio source. O’Dea et al. suggest that the “broad” component is associated with a bright $\text{H}\alpha$ nebula.

A detailed study of the optical spectrum from the central \sim kiloparsec of A 2597 by Voit & Donahue (1997) allowed them to measure the density, temperature and metal abundances of the line-emitting gas and conclude that the most likely explanation for the brilliant ionizing nebula in A 2597 is a population of hot stars. As a byproduct of their study they determine the redshift of PKS 2322–123 to be 0.0821 ± 0.0001 . HST observations by Koekemoer et al. (1998) reveal a series of blue knots and clumps that are most likely regions of recent star formation. They also find emission line filaments at the edges of the radio lobes, which argues for a direct interaction between the radio source and its environment. Falcke et al. (1998) recently detected molecular hydrogen in the central kiloparsecs of PKS 2322–123. They suggest that the luminous H_2 emission correlates with the presence of a strong radio source, luminous $\text{H}\alpha$ emission and a cooling flow of $>100 M_{\odot} \text{ y}^{-1}$.

We assume $H_0 = 75 \text{ km s}^{-1} \text{ Mpc}^{-1}$ and $q_0 = 0$ throughout.

2. VLBA Observations

The VLBA observations were carried out at 1.312 and 4.991 GHz with the 10-element VLBA and 27-element VLA of the NRAO⁴ in a single 10.5-hour observing session on 1996 December 7. The VLA was operated in “phased-array” mode to synthesize a single aperture with a large collecting area. The calibrator J2246-1206 was used to phase up the VLA every 25 minutes. The net integration time on PKS 2322–123 was 323 minutes at 1.3 GHz and 95 minutes at 5 GHz spread over multiple 19 minute snapshots to improve u,v coverage. Both right- and left-circular polarizations were observed with 2-bit sampling. The 1.3 and 5 GHz data were correlated in separate passes so as to provide high spectral resolution (1024 channels per 8 MHz wide IF band) without the RL and LR cross-correlation products at 1.3 GHz, and low spectral resolution (16 channels per IF band) with full cross-correlation products at 5 GHz.

Standard a priori flagging, amplitude calibration, fringe fitting, bandpass calibration (using 3C 84), and frequency averaging procedures were followed in AIPS. Global fringe fitting was performed on J2246-1206 and the resulting delays and rates were transferred to PKS 2322–123. Furthermore, after imaging, J2246-1206 was used in conjunction with CALIB to obtain time-dependent amplitude corrections which were also applied to A 2597. Subsequently, A 2597 was phase-only self-calibrated with a 1 minute solution interval. No amplitude self-calibration was performed on A 2597 itself. All manual editing, imaging, deconvolution, and self-calibration were performed using DIFMAP (Shepherd, Pearson, & Taylor 1994, 1995). Polarization calibration was performed on the 5 GHz data using J2246-1206 to determine the instrumental leakage terms, and the absolute polarization angle calibration was determined from a single 12 minute observation of 3C 286 which has known polarized structure (Cotton et al. 1997).

3. Continuum Results

In Fig. 1 we show the naturally weighted 1.3 and 5 GHz VLBA images. Both images display a clearly symmetric structure along a position angle of $\sim 70^\circ$. On kiloparsec scales a bright hot spot 0.5'' south-west of the nucleus (Sarazin et al. 1995) suggests some bending of the jet to a position angle of $\sim 50^\circ$. At the hot spot the south-west radio jet appears to be sharply deflected to the south, giving the large scale structure an overall “C” shape.

In the parsec scale jet at 1.3 GHz there are 5 components extended nearly in a line over 63 mas (89 pc) with the strongest component at the center. These components are labeled in Fig. 1, and parameterized by Gaussian modelfitting in Table 1. The central component is considerably stronger at 5 GHz and has a spectral index, α , of 0.6 ± 0.1 where $S_\nu \propto \nu^\alpha$. We identify this component as the core based on its inverted spectrum, compactness, strength, and the symmetric

⁴The National Radio Astronomy Observatory is operated by Associated Universities, Inc., under cooperative agreement with the National Science Foundation

morphology of the source. No significant polarized flux density was measured at 5 GHz above the noise floor of $40 \mu\text{Jy}/\text{beam}$. This indicates a fractional polarization of $<0.1\%$ for the nucleus, and $<10\%$ for components E2 and W2.

TABLE 1
COMPONENT FLUX DENSITIES AND SPECTRA

Component	r (mas)	θ ($^\circ$)	$S_{1.3\text{GHz}}$ (mJy)	$S_{5\text{GHz}}$ (mJy)	$\alpha_{1.3-5}$
E1	33	64	2.8 ± 0.5	< 0.2	< -1.9
E2	16	67	6.7 ± 0.6	4.8 ± 0.3	-0.25 ± 0.1
Core	0	0	16.6 ± 0.9	36.9 ± 1.9	$+0.60 \pm 0.1$
W2	16	-112	7.6 ± 0.6	4.1 ± 0.3	-0.47 ± 0.1
W1	30	-115	2.4 ± 0.5	< 0.2	< -1.9

A spectral index map of the nucleus of PKS 2322–123, made by tapering the 5 GHz image to the 1.3 GHz resolution, is shown in Fig. 2. The two images were aligned using the relatively steep spectrum component W2, rather than the core, because if the core component is the location in the jet where the synchrotron self absorption optical depth is unity, then its position will vary with frequency (Blandford & Königl 1979), such that higher frequencies look “deeper” down the jet towards the true center of activity. Also, a gradient in the free-free opacity towards the core may result in a shift in the apparent core location as a function of frequency. Given the low 5 GHz brightness temperatures for E2, C and W2 of 1.4×10^4 , $\sim 10^7$, and 1.2×10^4 K respectively, synchrotron self absorption is unlikely to be important. Higher frequency VLBI observations are needed to determine the intrinsic flux density and spectral index before the free-free optical depth, τ_{ff} , can be measured, but a rough estimate on τ_{ff} can be obtained by extrapolating the 5 GHz flux density to 1.3 GHz assuming a spectral index of -1 . This gives τ_{ff} of 1, 2.1 and 0.7 for E2, C and W2 respectively. These optical depths require emission measures of 7×10^7 , 14×10^7 , and $5 \times 10^7 \text{ cm}^{-3} \text{ pc}$ for E2, C and W2 assuming a gas temperature of 10^4 K (see Levinson, Laor, & Vermeulen 1995).

4. HI Absorption Results

In Fig. 3 we show the 1.3 GHz continuum emission and the spectra of each of the 5 components. Both a very broad (735 km s^{-1}) and a narrow (106 km s^{-1}) line are seen against the core component. Only the narrow line is seen against component E2, and neither line is detected towards W2. Measurements of the lines are given in Table 2 and shown graphically in Fig. 4. Both of these lines are significantly redshifted with respect to the velocity centroid of the optical emission lines from the nucleus. Voit & Donahue (1997) have obtained a high signal-to-noise

TABLE 2
HI COLUMN DENSITIES

Component (1)	$S_{1.3\text{GHz}}$ (2)	S_{line} (3)	V (4)	ΔV (5)	τ (6)	N_{H} (7)
E1 – narrow	2.8 ± 0.5	< 1.5 mJy	–	–	< 0.8	–
E2 – narrow	6.7 ± 0.6	3.1 ± 0.3	24882 ± 6	133 ± 14	0.63	12.2×10^{23}
Core – narrow	16.6 ± 0.9	2.3 ± 0.6	24880 ± 12	106 ± 33	0.15	2.3×10^{23}
W2 – narrow	7.6 ± 0.6	< 2.0 mJy	–	–	< 0.3	–
W1 – narrow	2.4 ± 0.5	< 1.5 mJy	–	–	< 1.0	–
E1 – broad	2.8 ± 0.5	< 1.0 mJy	–	–	< 0.5	–
E2 – broad	6.7 ± 0.6	< 1.0 mJy	–	–	< 0.2	–
Core – broad	16.6 ± 0.9	3.8 ± 0.3	24905 ± 19	735 ± 53	0.26	27.8×10^{23}
W2 – broad	7.6 ± 0.6	< 1.0 mJy	–	–	< 0.2	–
W1 – broad	2.4 ± 0.5	< 1.0 mJy	–	–	< 0.5	–

NOTES TO TABLE 2

Col.(1).—Component name and type of HI line detected (or upper limit given for). Col.(2).—Continuum flux density at 1.3 GHz in mJy. Col.(3).—Depth of the line in mJy or 3σ upper limit. Col.(4).—Central velocity in km s^{-1} . Col.(5).—FWHM in velocity in km s^{-1} . Col.(6).—Optical depth or 3σ upper limit. Col.(7).—The column density in units of cm^{-2} calculated assuming a covering factor of 1 and a spin temperature of 8000 K (Conway & Blanco 1995).

spectrum from which they derive an emission line redshift of $24613 \pm 60 \text{ km s}^{-1}$. The presence of large scale asymmetries in the emission line gas kinematics, however, may indicate that the gas is substantially offset from the systemic velocity. Stellar absorption features may better trace a more relaxed inner potential. Taking advantage of prominent Ca II H, K, and G band absorption features we performed a cross correlation analysis of the Voit & Donahue spectrum with a range of galaxy template spectra. Correlations with different spectra gave consistent results with a mean systemic velocity of $24673 \pm 20 \text{ km s}^{-1}$. Given the peculiar nature of PKS 2322–123 (elliptical with strong emission lines), which is not well matched to any of the templates, and the mismatch in spectral resolution, a more realistic error is $\pm 100 \text{ km s}^{-1}$. The mean offset of the HI absorption features from the systemic velocity is thus $220 \pm 100 \text{ km s}^{-1}$.

The broad (412 km s^{-1} FWHM) HI line centered at $24604 \pm 17 \text{ km s}^{-1}$ discovered by O’Dea et al. (1994) is not seen towards any component on the parsec scale. This is not surprising since it was spatially resolved, and appeared strongest towards the NE lobe of PKS 2322–123. In all likelihood the continuum and HI emission from the NE lobe has been resolved out. The narrow

(221 km s⁻¹ FWHM) spatially unresolved line seen by O’Dea et al. at 24886 ± 5 km s⁻¹ towards the nucleus is detected and spatially resolved by our observations.

The very broad (735 km s⁻¹ FWHM) line was not detected by O’Dea et al.. Its depth of 3.8 mJy should have been detectable by them even when diluted by unabsorbed emission within the beam, but given their poorer velocity coverage (1304 km s⁻¹ after editing) it is possible that this very broad line was lost in the continuum subtraction.

5. Discussion

5.1. Relation of Symmetric Structure to H I Absorption

The parsec scale structure of PKS 2322–123 appears extremely symmetric at both 1.3 and 5 GHz. If the jet components are intrinsically similar and were ejected from the core simultaneously, then either (1) the radio source must lie within a few degrees of the plane of the sky or (2) the bulk motion of the jets must be nonrelativistic. VLBI observations of two other FR-I radio galaxies embedded in X-ray cooling flow clusters (Hydra A – Taylor 1996; and 3C 338 – Feretti et al. 1993) have revealed remarkably symmetric structures on the parsec scale whereas over 95% of all AGN in complete flux limited samples have one-sided core+jet morphologies (Taylor et al. 1996). If even low power radio galaxies have jets that start out relativistic on parsec scales (Giovannini et al. 1998), then the jets of all 3 sources must be oriented with a few degrees of the plane of the sky. The chance of 3 out of 13 radio galaxies embedded in cooling flow clusters (see Taylor, Barton & Ge 1994) being within 5 degrees of the plane of the sky is $\sim 3\%$. Alternatively, it has been suggested (e.g., Soker & Sarazin 1988) that cooling flows may decelerate the radio jets, although such disruption has been considered to occur at the sonic radius (where the inflow velocity exceeds the sound speed) somewhere between 0.1–10 kpc. Unless the cooling flows have an affect on the jet closer to the nucleus than previously thought it is difficult to understand why the parsec scale jets in Hydra A, 3C 338, and PKS 2322–123, would have such low bulk velocities.

Examination of the parsec scale structure of sources with H I detected in absorption (Hydra A – Taylor 1996; 1413+135 – Perlman et al. 1996; N 3894 – Peck & Taylor 1998; 1946+708 – Peck, Taylor, & Conway 1999) indicates that a symmetric parsec-scale structure correlates strongly with the presence of H I, although there are counter-examples (e.g. Mrk 231 – Carilli, Wrobel & Ulvestad 1998). 3C 84 could be an intermediate case – observations by Vermeulen et al. (1994) suggest an inclination of $\sim 45^\circ$. The most likely explanation for this correlation is that symmetric sources are oriented close to the plane of the sky such that their appearance is not made one-sided by Doppler boosting effects. This then provides a favorable viewing angle of the radio source through a disk or torus of atomic gas that is perpendicular to the jet axis. This picture is consistent with unified schemes, and our limited understanding of how the central engine in AGN might be fed.

In the inner regions of the disk a large fraction of the gas must be ionized by the central

engine. This will result in free-free absorption of the radio continuum at frequencies below ~ 5 GHz as seen in 3C 84 (Walker et al. 1998), Hydra A (Taylor 1996), 1946+708 (Peck et al. 1999), and PKS 2322–123. Another result of the dense ionized gas, if magnetized, could be extremely high Faraday rotation measures (RMs). Owing to the lack of any polarized flux in these systems, it has not been possible to directly measure the RMs in any source with HI absorption, but the presence of very high RMs could explain why no polarized flux is detected from these sources.

5.2. Location of the Atomic Gas

The sharp spatial variations in optical depth on scales of order 10 pc (Fig. 4), and the detection of the very broad line only against the core, argue that the atomic gas we are seeing is located in the central 10s of parsecs of PKS 2322–123, and is not just a chance encounter with a cloud in the galaxy. If the gas is distributed in a disk centered on the core then it must be fairly thin (< 20 pc) so as to cover the core and E2, but not W2. This situation is somewhat different from the radio galaxy 1946+708 (Peck et al. 1999) where HI gas is seen across the entire 60 parsec extent of the radio source. However, in 1946+708 as in PKS 2322–123, a broad component (~ 300 km s $^{-1}$ wide) is seen only within ~ 10 pc of the core. The 735 km s $^{-1}$ FWHM line in PKS 2322–123 is, to our knowledge, the broadest HI absorption line, and is considerably wider than the optical emission lines from the nucleus of PKS 2322–123 which have a velocity dispersion of 270 km s $^{-1}$ (Voit & Donahue 1997) albeit from much lower spatial resolution observations.

The fact that both lines in PKS 2322–123 are redshifted by $\sim 220 \pm 100$ km s $^{-1}$ may imply that the gas is in-falling. This is similar to the trend found by van Gorkom et al. (1989) for 6 of 8 HI absorption systems in a sample of nearby ellipticals. If this gas is in a disk, then the disk is not in an orderly Keplerian rotation about the nucleus, but has significant inward streaming motions. From the very broad linewidths, much broader than the thermal linewidths for any plausible conditions, we can also infer considerable velocity structure in the disk, probably due to turbulence. Alternatively, given the velocity offset of the very broad line from the absorption line redshift of 232 ± 100 km/s, it is possible that the very broad line is at the systemic velocity. In this case it would be natural to explain the linewidth by rotation. Unfortunately, we don't know the radial extent of the disk since that is perpendicular to the radio axis. Assuming a radius of 10 pc, the mass required to produce the observed linewidth is $2 \times 10^8 M_{\odot}$.

GBT thanks STScI for hospitality during a visit in which this paper was written. This research has made use of the NASA/IPAC Extragalactic Database (NED) which is operated by the Jet Propulsion Laboratory, Caltech, under contract with NASA.

REFERENCES

- Blandford, R. D., & Königl, A. 1979, *ApJ*, 232, 34
- Carilli, C. L., Wrobel, J. M., & Ulvestad, J. S. 1998, *AJ*, 115, 928
- Conway, J. E., & Blanco, P. R. 1995, *ApJ*, 449, L131
- Crane, P. C., van der Hulst, J. M., & Haschik, A. D. 1982, in proceedings of IAU Symposium No. 97, *Extragalactic Radio Sources*, eds. D. S. Heeschen & C. M. Wade, (Dordrecht, Reidel), 307
- Cotton, W. D., Fanti, C., Fanti, R., Dallacasa, D., Foley, A. R., Schilizzi, R. T., & Spencer, R. E. 1997, *A&A*, 325, 479
- Dwarakanath, K. S., van Gorkom, J. H., & Owen, F. N. 1994, *ApJ*, 432, 469
- Dwarakanath, K. S., Owen, F. N., & van Gorkom, J. H. 1995, *ApJ*, 442, L1
- Falcke, H., Rieke, M. J., Rieke, G. H., Simpson, C., & Wilson, A. S. 1998, *ApJ*, 494, L155
- Feretti, L., Comoretto, G., Giovannini, G., Venturi, T., & Wehrle, A. E. 1993, *ApJ*, 408, 446
- Giovannini, G., Taylor, G. B., Arbizzani, E., Bondi, M., Cotton, W. D., Feretti, L., Lara, L. & Venturi, T. 1998, in preparation
- van Gorkom, J. H., Knapp, G. R., Ekers, R. D., Ekers, D. D., Laing, R. A., & Polk, K. S. 1989, *AJ*, 97, 708
- Jaffe, W. 1990, *A&A*, 240, 254
- Jaffe, W. 1991, *A&A*, 250, 67
- Koekemoer, A. M. et al. 1998, in preparation
- Levinson, A., Laor, A., & Vermeulen, R.C. 1995, *ApJ*, 448, 589
- O’Dea, C. P., Baum, S. A., & Gallimore, J. F. 1994, *ApJ*, 436, 669
- O’Dea, C. P., Gallimore, J. F., & Baum, S. A. 1995, *AJ*, 109, 26
- Peck, A. B., & Taylor, G. B. 1998, *ApJ*, 502, L23
- Peck, A. B., Conway, J. E., & Taylor, G. B. 1999, in prep.
- Perlman, E. S., Carilli, C. L., Stocke, J. T., & Conway, J. E. 1996, *AJ*, 111, 1839
- Sarazin, C. L., Burns, J. O., Roettiger, K., & McNamara, B., 1995, *ApJ*, 447, 559
- Shepherd, M. C., Pearson, T. J., & Taylor, G. B. 1994, *BAAS*, 26, 987
- Shepherd, M. C., Pearson, T. J., & Taylor, G. B. 1995, *BAAS*, 27, 903
- Soker, N., & Sarazin, C. L. 1988, *ApJ*, 327, 66
- Taylor, G. B., Barton, E. J., & Ge, J.-P. 1994, *AJ*, 107, 1942
- Taylor, G. B. 1996, *ApJ*, 470, 394

- Taylor, G. B., Vermeulen, R. C., Readhead, A. C. S., Pearson, T. J., Henstock, D. R., & Wilkinson, P. N. 1996, in “The Second Workshop on Gigahertz Peaked Spectrum and Compact Steep Spectrum Radio Sources”, eds. I.A.G. Snellen, R.T. Schilizzi, H.J.A. Rottgering, and M.N. Bremer (Leiden Observatory:Leiden), p. 263
- Vermeulen, R. C., Readhead, A. C. S., & Backer, D. C. 1994, ApJ, 430, L41
- Voit, G. M., & Donahue, M. 1997, ApJ, 486, 242
- Walker, R. C., Kellermann, K. I., Dhawan, V., Romney, J. D., Benson, J. M., Vermeulen, R.C., & Alef, W. 1998, in *IAU Colloquium 164: Radio Emission from Galactic and Extragalactic Compact Sources* eds. J. A. Zensus, G. B. Taylor and J. M. Wrobel (PASP: San Francisco) Vol. 144, p. 133
- White, D. A., Fabian, A. C., Johnstone, R. M., Mushotzky, R. F. & Arnaud, K. A. 1991, MNRAS, 252, 72

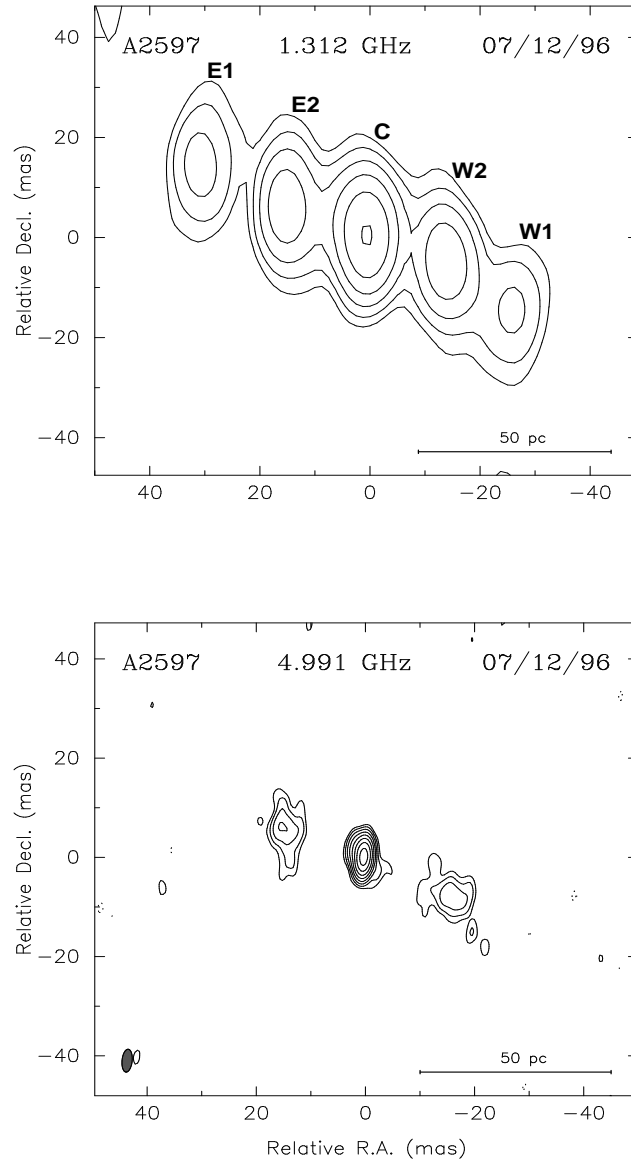


Fig. 1.— The naturally weighted images of PKS 2322–123 at 1.3 and 5 GHz. The restoring beam has dimensions 16.3×6.7 mas in position angle -1.3° at 1.3 GHz and 4.63×1.86 mas in position angle -5.1° at 5 GHz. Contours are at factor 2 intervals and start at 0.5 and 0.2 mJy/beam for the 1.3 and 5 GHz images respectively.

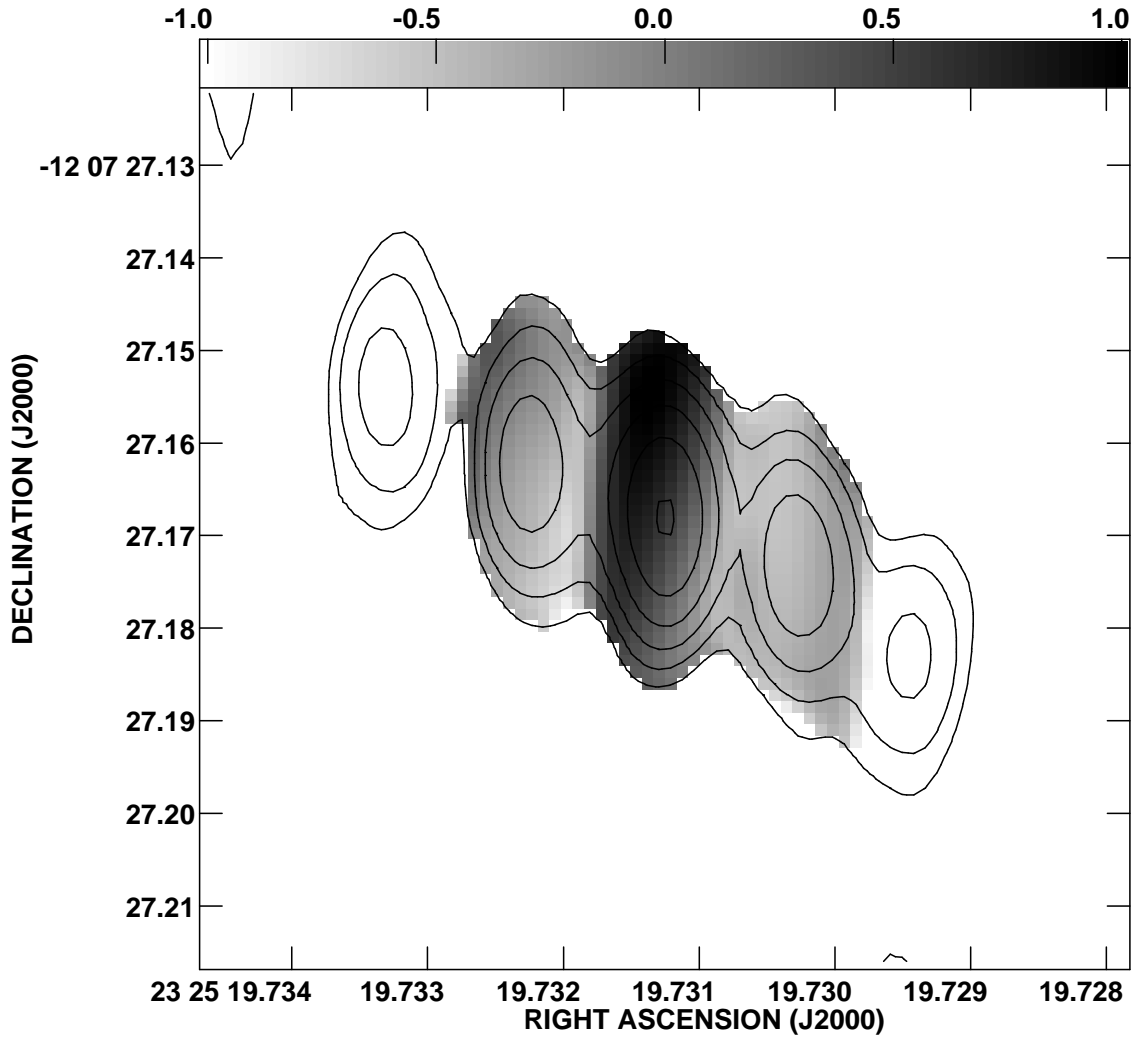


Fig. 2.— A spectral index map of PKS 2322–123 between 1.3 and 5 GHz with 1.3 GHz contours overlaid. The 5 GHz image has been heavily tapered and restored to the same resolution as the 1.3 GHz image. The images have been registered using component W2.

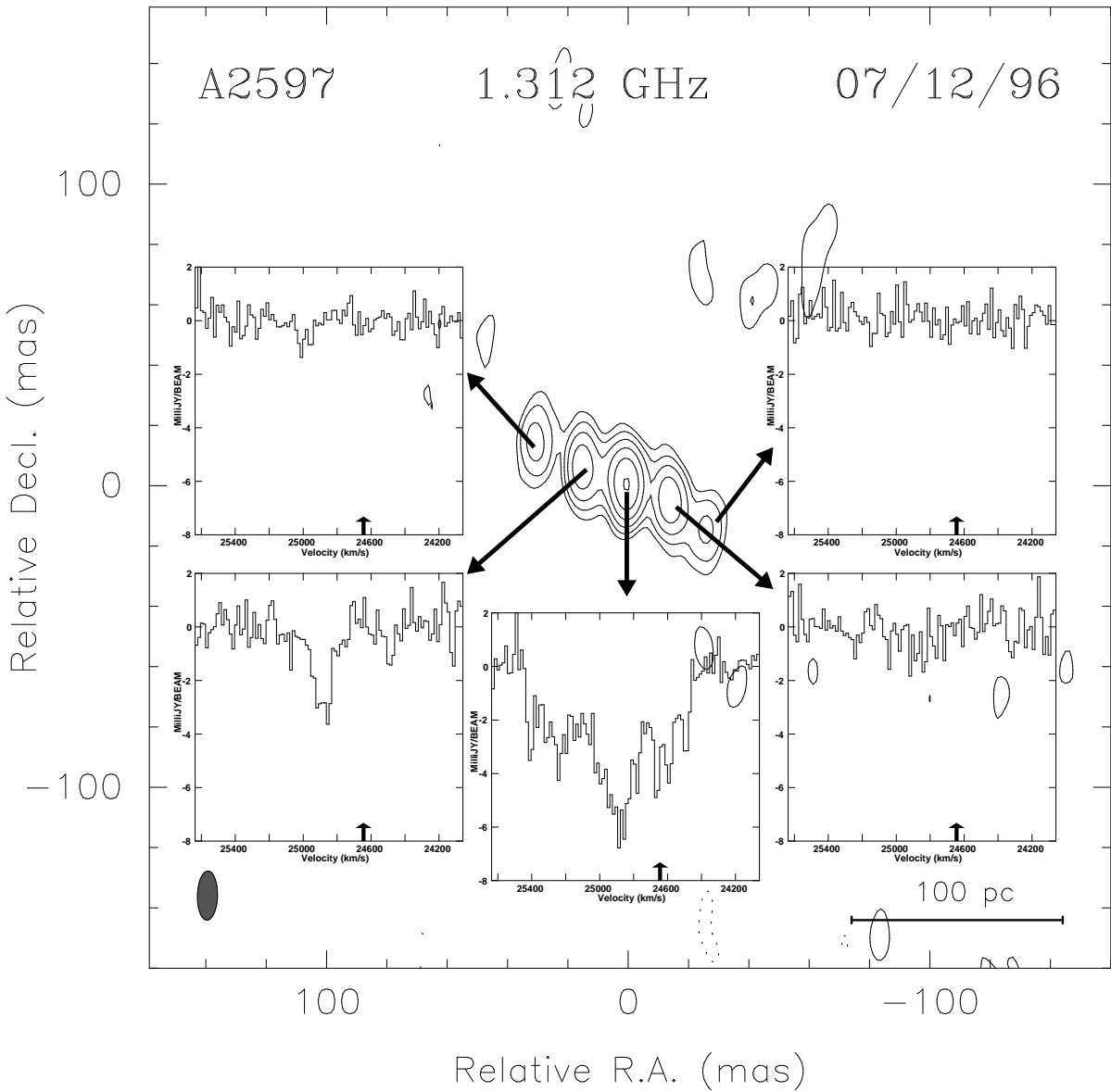


Fig. 3.— The 1.3 GHz continuum image from Fig. 1 with the spectra for each of the 5 components overlaid. The velocity resolution is 7.1 km s^{-1} . The arrow at 24673 km s^{-1} indicates the systemic velocity derived from the optical redshift as discussed in the text and the width of the arrowhead represents the 1σ uncertainty of 100 km s^{-1} .

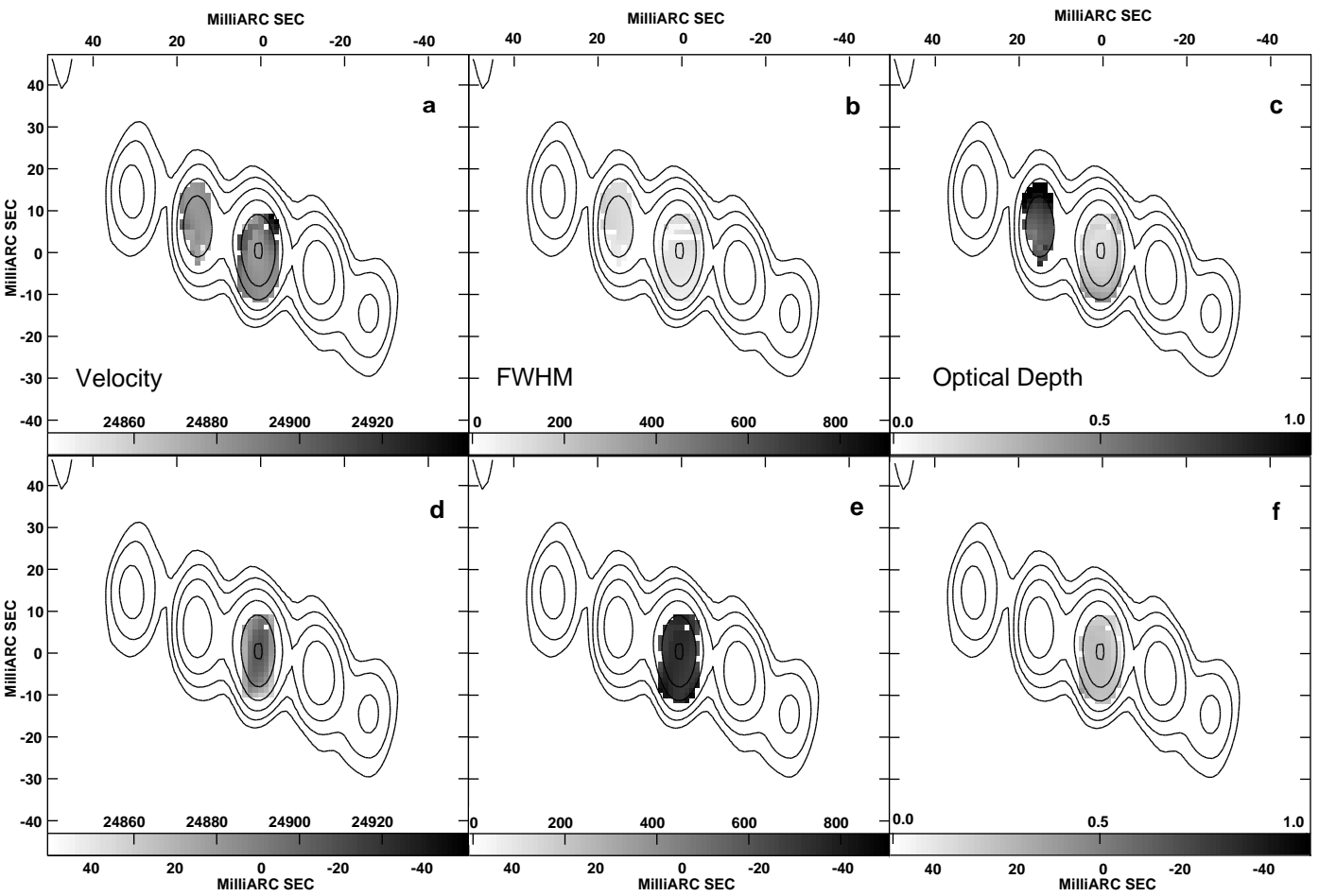


Fig. 4.— Optical depth (τ), velocity (km s^{-1}) and FWHM (km s^{-1}) grayscale plots obtained by fitting 1 dimensional Gaussians to the HI spectra pixel by pixel. No fit was attempted in the absence of 3 channels with 1.5 mJy or more of absorption. The top row is for the narrow component and the bottom row is for the broad component.